Chemical Engineering Journal 148 (2009) 279–289

Contents lists available at ScienceDirect

Chemical Engineering Journal

journal homepage: www.elsevier.com/locate/cej

Hydrodynamics of tapered anaerobic fluidized beds for metabolic gas production

Chun-Sheng Wu [a,*], Ju-Sheng Huang [b], Reiko Ohara [c]

[a] Department of Resources and Environment, Leader University, Tainan City 709, Taiwan, ROC
[b] Department of Environmental Engineering, Kun Shan University, Tainan County 710, Taiwan, ROC
[c] Energy & Environment Laboratories, Industrial Technology Research Institute, Chutung, Hsinchu County 310, Taiwan, ROC

ARTICLE INFO

Article history:
Received 10 March 2008
Received in revised form 20 August 2008
Accepted 25 August 2008

Keywords:
Tapered anaerobic fluidized bed
Hydrodynamics
Metabolic gas production
Modeling

ABSTRACT

A laboratory study using two tapered anaerobic fluidized bed reactors (AFBRs) with taper angles (θ) of 2.5° and 5° was undertaken to explore the hydrodynamic behavior of AFBRs during metabolic gas production. Predictive models were formulated to describe the hydrodynamic behavior of tapered AFBRs in a way that accounted for wake theory, hydrostatic pressure, biofilm thickness distribution, and ambient temperature. When the two tapered AFBRs were maintained in their respective fully fluidized states, both the measured and simulated three-phase bed heights, $H_{b,GLS}$, were higher than the corresponding two-phase bed heights, $H_{b,LS}$—a bed-expansion effect. In contrast, the measured and simulated three-phase bed-pressure gradient $(-\Delta P_t/V_b)_{GLS}$, was lower than the corresponding two-phase value $(-\Delta P_t/V_b)_{LS}$, especially at higher superficial liquid (u_l) and gas velocities (u_g). This helped to thicken the biofilm. Increasing θ from 2.5° to 5°, decreased $H_{b,GLS}$ sufficiently to offset increases in $(1-\varepsilon_f)$. Consequently, the values of both $(-\Delta P_{flu})_{GLS}$ and $(-\Delta P_t/V_b)_{GLS}$ decreased. The simulated values for $H_{b,GLS}$ and $(-\Delta P_t/V_b)_{GLS}$ were in fairly good agreement with experimental results. Compared to conventional AFBRs, the effect of metabolic gas production on the expansion behavior of tapered AFBRs was smaller. Thus, tapering of AFBRs facilitates the development of thick biofilms.

1. Introduction

In a conventional anaerobic fluidized bed reactor (AFBR) of constant cross-sectional area, a bioparticle is in a dynamic, fully fluidized equilibrium in which the upward drag force is balanced by the negative buoyant force from gravity. In a tapered AFBR, in contrast, both the superficial velocity and the upward drag force vary with depth within the bioreactor, resulting in either a partially fluidized or a fully fluidized state. In practice, the geometric properties of tapered AFBRs—the wider cross-sectional area and greater height result in reduced superficial velocity and upward drag force at the upper part of the AFBR, can mitigate the washout of bioparticles from bioreactors [1].

In the past, research on the hydrodynamics of three-phase fluidized beds with applications in chemical engineering commonly used external gas injection to simulate the gas phase [2–5]. A few studies on the hydrodynamics of biological fluidized beds also used external gas injection [6,7]. Studies on the hydrodynamics of anaerobic fluidized beds (AFBs) showing metabolic gas production have been scarce [8,9], especially studies involving tapered AFBs. Huang and Wu [10] demonstrated that steady-state biofilm thickness varies inversely with the specific energy dissipation rate (i.e., the energy dissipation per unit volume of bioreactor per unit time, ω). Together with the superficial liquid velocity (u_l), the bed-pressure gradient ($(-\Delta P_t/V_b)_{GLS}$) is one of the most influential parameters determining the value of ω. In addition, the three-phase bed volume ($V_{b,GLS}$) is a function of the three-phase bed height ($H_{b,GLS}$), which is closely related to the bioparticle washout rate [1].

The hydrodynamics of AFBs generally vary with changes in the gas, liquid, and solid hold-ups. Most researchers accept a generalized wake model that takes into account the mean volume ratio of wakes to bubbles (k) and the ratio of the solid fraction in a liquid wake to that in the liquid–solid fluidization phase (x) [2]. Hence, many researchers have focused their attention on deriving equations for correlating k and/or x. A wake model for conditions when $x=0$ (i.e., when the liquid wakes are particle-free) was developed, and this model effectively approximates systems with large or dense particles [3–5,8,9]. A recent modeling approach for the simulation of bed expansion was proposed that adopts a correlation equation for liquid hold-up [11,12]. Yu and Rittmann [13] developed a bed-expansion model for the three-phase AFBR that combines the wake model with a correlation equation for gas

* Corresponding author. Tel.: +886 6 2552607; fax: +886 6 2551659.
E-mail address: wujoe38@mail.leader.edu.tw (C.-S. Wu).

1385-8947/$ – see front matter © 2008 Elsevier B.V. All rights reserved.
doi:10.1016/j.cej.2008.08.030

Nomenclature

A	cross-sectional area (cm^2)
AFB	anaerobic fluidized bed
AFBR	anaerobic fluidized bed reactor
b	bed width (cm)
d	diameter (cm)
D	equivalent diameter (cm)
Ga	Galileo number = $\rho_l d_p{}^3(\rho_p - \rho_l)g/\mu_l{}^2$
H	height (cm)
H_c	axial distance from reactor bottom to reactor top (cm)
H_0	axial distance from reactor bottom to its hypothetical apex = $b_0/(2\tan\theta_1)$ (cm)
H^*	dimensionless height of a certain cross-section of the TAFBR = H/H_b
HRT	hydraulic retention time (h)
k	mean volume ratio of wakes to bubbles
m	linear proportion constant for Eq. (14) (cm)
M_m	mass of carriers (g)
n	bed-expansion index
P	pressure ($dyn\,cm^{-2}$)
P_{atm}	atmospheric pressure = 1,013,962 ($dyn\,cm^{-2}$)
Q	flow rate ($cm^3\,s^{-1}$)
S	substrate concentration (mg acetate l^{-1})
T	temperature (°C)
TAFBR	tapered anaerobic fluidized bed reactor
u	superficial velocity ($cm\,s^{-1}$)
u_t	terminal settling velocity of a particle without wall effect ($cm\,s^{-1}$)
V	volume (cm^3)
VLR	volumetric loading rate ($g\,acetate\,l^{-1}\,d^{-1}$) = $Q_i S_i/V_{b,GLS}$
v_i	terminal settling velocity of a particle with wall effect = $u_t 10^{-d_p/D}$ ($cm\,s^{-1}$)
x	ratio of solid fraction in a liquid wake to that in the liquid–solid fluidization phase
Z	axial distance from a certain cross-section of TAFBR to its hypothetical apex (cm)

Greek letters

δ	biofilm thickness (cm)
ε	hold-up
ϕ^2	Thiele modulus
μ	dynamic viscosity ($dyn\,s\,cm^{-2}$)
θ	taper angle (°)
θ_1	half taper angle = $\theta/2$ (°)
ρ	density ($g\,cm^{-3}$)

Subscripts

0	bottom
1	top
a	average
atm	atmosphere
b	bed
c	certain cross-section
bf	biofilm
d	dry
f	fluid
flu	fluidized
g	gas
GLS	gas–liquid–solid
i	inflow
LS	liquid–solid
l	liquid
m	media (carrier)
mf	minimum fluidization
p	particle
r	recirculation
t	total
tr	transport
u	unfluidized
w	wet

hold-up, adjustments for terminal settling velocity, and their own correlation equations for k.

In an AFBR designed for metabolic gas production, the hydrostatic pressure at the bottom of the fluidized bed is higher than at the top of the fluidized bed. According to Boyle's law, which states that the volume of a gas varies inversely with its pressure at constant temperature, the bubbles of metabolic gas gradually increase in size as they rise within the bioreactor. Thus, the gas, liquid, and solid hold-ups vary with height within the fluidized bed. In addition, the operating temperature of the AFBR frequently differs from the ambient temperature, and such a temperature difference must be taken into account in order to calculate the most accurate values possible for the gas volume (via Charles' law) and the gas hold-up. Furthermore, the biofilm thickness, which varies along the length of the bioreactor [1,6], directly influences the solid, liquid, and gas hold-ups.

In this work, a laboratory study using two tapered AFBRs with taper angles (θ) of 2.5° and 5° was undertaken to explore the hydrodynamics of tapered AFBs during metabolic gas production. Hydrodynamic models for the three-phase bed height, $H_{b,GLS}$, and the three-phase pressure gradient $(-\Delta P_t/V_b)_{GLS}$, were formulated by taking into account wake theory, hydrostatic pressure, biofilm thickness distributions, and ambient temperature. In an attempt to unravel the effects of superficial liquid velocity, u_l, and metabolic gas production (i.e., superficial gas velocity, u_g) on the hydrodynamic behavior of tapered AFBRs, experimental measurements and model simulations of the three-phase reactor operating parameters $H_{b,GLS}$ and $(-\Delta P_t/V_b)_{GLS}$ were compared with the corresponding parameters of the two-phase system, $H_{b,LS}$ and $(-\Delta P_t/V_b)_{LS}$.

2. Theory and model formulation

2.1. Wake model, terminal settling velocity, and bioparticle characteristic parameters

In the present study, large bioparticles (approximately d_p = 1000 μm) were observed in both tapered AFBRs. Thus, the generalized wake model was simplified by setting $x = 0$ [3,8,9,13], as shown in the following equation:

$$\varepsilon_{l,GLS} = \left(\frac{u_l - k u_g}{v_i}\right)^{1/n} (1 - \varepsilon_g - k\varepsilon_g)^{1-(1/n)} + k\varepsilon_g \quad (1)$$

If both u_g and ε_g are set zero, Eq. (1) can be simplified to Eq. (2):

$$\varepsilon_{l,LS} = \left(\frac{u_l}{v_i}\right)^{1/n} \quad (2)$$

The following correlation equations for n and u_t, proposed by Khan and Richardson [14,15], were applied to yield Eqs. (3) and (4):

$$\frac{4.8 - n}{n - 2.4} = 0.043\mathrm{Ga}^{0.57}\left[1 - 1.24\left(\frac{d_p}{D}\right)^{0.24}\right] \quad (3)$$

$$u_t = \frac{\mu_l}{\rho_l d_p}(2.33\mathrm{Ga}^{0.018} - 1.53\mathrm{Ga}^{-0.016})^{13.3} \quad (4)$$

ρ_p can then be calculated using by the following equation (5) [8,9]:

$$\rho_p = \frac{\rho_{mw} + \rho_{bf}[(1+(2\delta/d_m))^3 - 1]}{(1+(2\delta/d_m))^3} \quad (5)$$

thetical TAFB apex (Z_u, Z_{tr}) can be calculated using Eqs. (8) and (9), respectively [10]:

$$Z_u = \frac{1}{2\ \tan\theta_1}\left(\frac{Q_i + Q_r}{u_{mf}}\right)^{1/2} \quad (8)$$

$$Z_{tr} = \frac{1}{2\ \tan\theta_1}\left(\frac{Q_i + Q_r}{v_i}\right)^{1/2} \quad (9)$$

where u_{mf} can be calculated using Eq. (10) [10]:

$$u_{mf} = \mu_l \left\{ \frac{[(150(1-\varepsilon_{mf})/\varepsilon_{mf}^3)^2 + 4\mathrm{Ga}(1.75/\varepsilon_{mf}^3)]^{1/2} - 150(1-\varepsilon_{mf})/\varepsilon_{mf}^3}{2\rho_l d_p \times 1.75/\varepsilon_{mf}^3} \right\} \quad (10)$$

2.2. Gas hold-up

The following correlation equation for ε_g, proposed by Buffière et al. [16], was applied:

$$\varepsilon_g = 0.239 d_p^{0.168} u_g^{0.70} \quad (6)$$

All individual hold-up coefficients must sum to unity, as shown in Eq. (7):

$$\varepsilon_g + \varepsilon_{l,GLS} + \varepsilon_{p,GLS} = 1 \quad (7)$$

2.3. Bed expansion, biofilm thickness distribution, and temperature correction

A schematic of the tapered AFB (TAFB) is presented in Fig. 1. The heights of the unfluidized and transport zones above the hypo-

$V_{b,GLS}$ and V_p can then be calculated using Eqs. (11) and (12), respectively:

$$V_{b,GLS} = \frac{4}{3}\tan^2\ \theta_1[(H_{b,GLS} + H_0)^3 - H_0^3] \quad (11)$$

$$V_p = \frac{M_m}{\rho_{md}((\pi/6)d_m^3)}\frac{\pi}{6}(d_m + 2\delta)^3 = \frac{M_m}{\rho_{md}}\left(1 + \frac{2\delta}{d_m}\right)^3 \quad (12)$$

The correlation equation relating $\varepsilon_{l,GLS}$, ε_g, and V_p is expressed as follows:

$$V_p = 4\ \tan^2\theta_1 \int_{H_0}^{H_0+H_b} (1-\varepsilon_f)Z^2\ dZ \quad (13)$$

where ε_f ($=\varepsilon_{l,GLS} + \varepsilon_g$) represents the fluid hold-up. The value of δ increases with the bed height in a tapered AFBR [1], and a linear

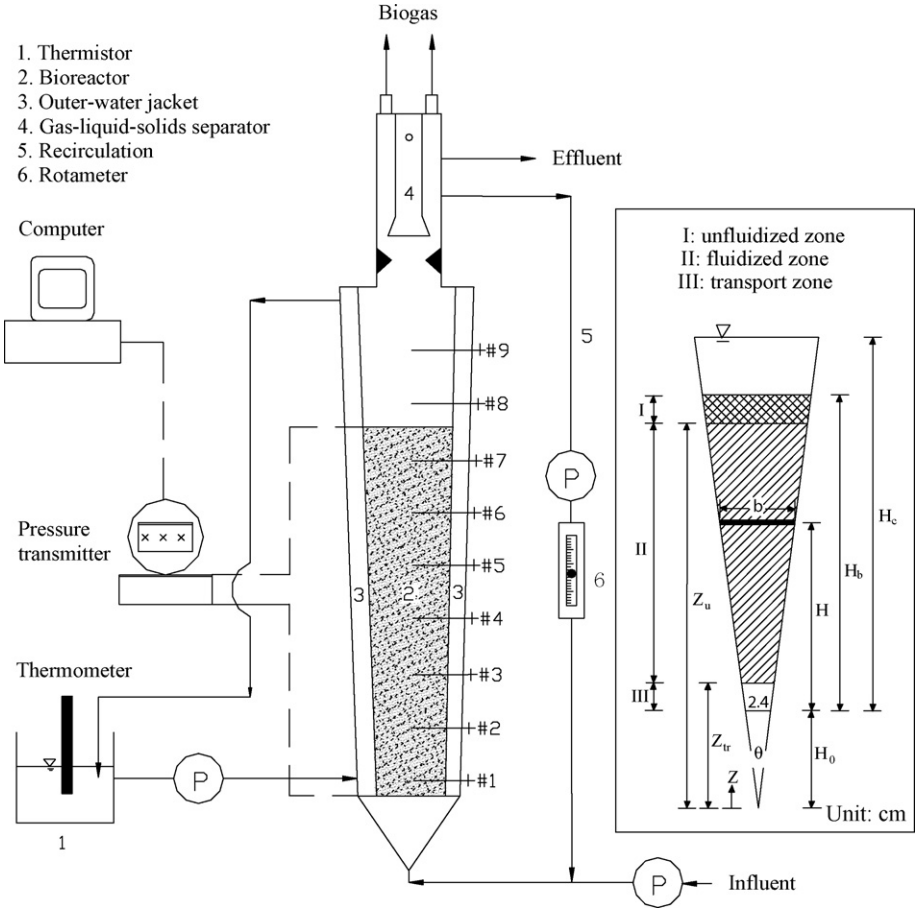

Fig. 1. Schematic diagram of tapered fluidized bed bioreactor system.

relationship relating δ to bed height can be assumed, as shown in the following equation:

$$\delta = \delta_0 + \mathrm{mH}* \tag{14}$$

By combining Boyle's and Charles' laws, an equation can be derived for the metabolic gas production rate at position H that takes into account temperature deviations (Eq. (15)):

$$Q_g = \frac{P_{atm}}{P_{atm} + \rho_l g(H_c - H)} \frac{273.2 + T_c}{273.2 + T_a} Q_{ga} \tag{15}$$

The average $\varepsilon_{l,GLS}$ and ε_g of the TAFBR can then be calculated using Eqs. (16) and (17), respectively:

$$\varepsilon_{l,GLS,a} = \frac{4\ \tan^2\theta_1}{V_{b,GLS}} \int_{H_0}^{H_0+H_b} \varepsilon_{l,GLS} Z^2\ \mathrm{d}Z \tag{16}$$

$$\varepsilon_{g,a} = \frac{4\tan^2\theta_1}{V_{b,GLS}} \int_{H_0}^{H_0+H_b} \varepsilon_g Z^2\ \mathrm{d}Z \tag{17}$$

The equation relating V_p to $V_{b,GLS}$ is as follows:

$$V_p = V_{b,GLS}(1 - \varepsilon_{l,GLS,a} - \varepsilon_{g,a}) = V_{b,GLS}(1 - \varepsilon_{f,a}) = V_{b,GLS}\varepsilon_{p,a} \tag{18}$$

The equivalent diameter (D) of the TAFBR can be calculated from the following equation:

$$D = \frac{4\tan\theta_1}{\sqrt{\pi}}(H_0 + H) \tag{19}$$

2.4. Bed-pressure gradient

The pressure drop across the transport zone is very low and can therefore be neglected. The pressure drops across both the unfluidized and fluidized zones can be calculated using Eqs. (20) and (21), respectively [17]:

$$(-\Delta P_u)_{GLS} = \int_{Z_u}^{Z_1} \left[150 \frac{(1-\varepsilon_{mf})^2}{\varepsilon_{mf}^3} \frac{\mu_l u_f}{d_p^2} + 1.75 \frac{1-\varepsilon_{mf}}{\varepsilon_{mf}^3} \frac{\rho_f u_f^2}{d_p} \right] \mathrm{d}Z \tag{20}$$

$$(-\Delta P_{flu})_{GLS} = g \int_{Z_{tr}}^{Z_u} (1 - \varepsilon_f)(\rho_p - \rho_f)\mathrm{d}Z \tag{21}$$

where ρ_f is determined by Eq. (22) [9]:

$$\rho_f = \frac{\varepsilon_{l,GLS}\rho_l + \varepsilon_g \rho_g}{\varepsilon_{l,GLS} + \varepsilon_g} \tag{22}$$

Peng and Fan [17] developed a modified form of the equation for the kinetic pressure drop ($(-\Delta P_k)_{GLS}$), which is given in the following equation:

$$(-\Delta P_k)_{GLS} = \frac{1}{2}\left[\rho_{f1} \left(\frac{u_{f1}}{\varepsilon_{f1}} \right)^2 - \rho_{f0} \left(\frac{u_{f0}}{\varepsilon_{f0}} \right)^2 \right] \tag{23}$$

Thus, the pressure drop $(-\Delta P_t)_{GLS}$ can be expressed as follows:

$$(-\Delta P_t)_{GLS} = (-\Delta P_u)_{GLS} + (-\Delta P_{flu})_{GLS} + (-\Delta P_k)_{GLS} \tag{24}$$

The bed-pressure gradient $(-\Delta P_t/V_b)_{GLS}$ can then be written in the following manner:

$$\left(\frac{-\Delta P_t}{V_b} \right)_{GLS} = \left(\frac{(-\Delta P_t)_{GLS}}{V_{b,GLS}} \right) \tag{25}$$

Similarly $(-\Delta P_t)_{LS}$, and $(-\Delta P_t/V_b)_{LS}$ can be calculated by applying Eqs. (11) and (20)–(25), with ε_g and u_g set to 0 and $H_{b,LS}$ replacing $H_{b,GLS}$ in Eq. (11).

3. Materials and methods

3.1. Tapered AFBRs

Two models of tapered AFBR made from Plexiglas with $\theta = 2.5^\circ$ and 5° were used. The two tapered AFBRs (working volume = 4.0 L each) had the same bed width at the bottom (2.4 cm), but different bed widths at the top (8.0 and 10.3 cm), as well as different bed heights (129.5 and 89.5 cm). The dimensions of the gas–liquid–solid separator, which was positioned at the top of the reactor, were 6.0 cm (length) × 6.0 cm (width) × 18.7 cm (height). The temperature of the TAFBR, which was equipped with a liquid flow meter and the metabolic gas collection apparatus, was maintained at 35 ± 1 °C by circulating hot water through the outer water-jacket.

3.2. Operation of tapered AFBR system

Samples of granulated activated carbon (200 g) were loaded into each tapered AFBR. The average carbon granule was 633 μm in diameter, and the diameters of the 10th and 60th percentiles were 383 and 667 μm, respectively. Granules had a dry density of 1.37 g cm^{-3}, and a wet density of 1.57 g cm^{-3}. The TAFBRs were then seeded with acclimated anaerobic sludge, which was obtained from an up-flow anaerobic sludge bed reactor. The TAFBRs were used to treat synthetic acetate wastewater with the following composition: 2500 mg acetate l^{-1}, 40 mg yeast extract l^{-1}, 1000 mg NaH_2PO_4 l^{-1}, 400 mg NH_4Cl l^{-1}, trace metals Ni^{+2}, Fe^{+3}, Co^{+2}, Mo^{+6}, Zn^{+2}, Mn^{+2}, and Mg^{+2} at 0.5 mg l^{-1} each, acidified to pH 6.0 by the addition of concentrated HCl (0.4 ml l^{-1}). The liquid recycle rate was adjusted to maintain the bioparticles in the fluidization state [10]. The reactor was semi-continuously fed with acetate (i.e., 4 l of synthetic acetate wastewater filled and drawn daily) for 1 week, and was run in operating mode continuously for three months. Afterwards, six test runs in which the volumetric loading rates were between 38.5–72.1 g-acetate l^{-1} d^{-1} were conducted using the two tapered AFBRs (Table 1). Each of these tests was run continuously for two months. The tapered AFBRs were assumed to have reached pseudo-steady state when the effluent acetate concentration deviated by less than 10% in three consecutive samples taken at a sampling rate of twice per week. Image analysis methods were used to determine d_p [18], and δ was determined using the method outlined by Shieh et al. [19]. Values for ρ_{mw} and ρ_{bf} were obtained according to the method of Huang and Wu [10]. The bed height was measured with ruler and recorded. Metabolic gas samples were collected with

Table 1
Operating conditions for three-phase tapered AFBRs

Run	θ (°)	Q_i (l d^{-1})	S_i (mg acetate l^{-1})	Q_r (l min^{-1})	VLR[a] (g acetate l^{-1} d^{-1})	u_{l0} (cm s^{-1})	u_{g0} (cm s^{-1})
1	2.5	10	2500	0.8	38.5	2.34	0.0209
2	2.5	20	2500	1.0	43.0	2.93	0.0428
3	2.5	20	5000	1.2	63.3	3.51	0.0838
4	5.0	10	2500	0.9	44.1	2.62	0.0207
5	5.0	20	2500	0.9	72.1	2.64	0.0412
6	5.0	20	5000	1.2	65.2	3.51	0.0838

[a] Volumetric loading rate.

Table 2
Operation conditions of hydrodynamic experiments for three-phase tapered AFBRs

Run	θ (°)	u_{l0}[a] (cm s^{-1})	u_{g0}[b] (cm s^{-1})	δ (μm)
1	2.5	1.47–7.83	0.0209	38
2	2.5	2.93–7.56	0.0428	73
3	2.5	3.51–14.51	0.0838	146
4	5.0	1.47–7.25	0.0207	39
5	5.0	2.64–7.27	0.0412	55
6	5.0	3.51–10.17	0.0838	83

[a] Exact values as shown in Fig. 2.
[b] $u_{g0} = 0$ for without metabolic gas production.

gas-collection bags and were used to determine Q_{ga}. A gas chromatographic column system (Schimadzu, model GC-14A) was used to measure acetate, CH_4 and CO_2. Acetate was measured with use of a 150 cm × 0.53 mm Supleco-Nikol fused-silica capillary column, a flame ionization detector, nitrogen carrier gas, injector and detector maintained at 230 °C. CH_4 and CO_2 content were measure with the use of a 150 cm × 3 mm stainless-steel column packed with Porapak Q 50/80 and Porapak T 50/80, a thermal conductivity detector, helium carrier gas, injector and detector, respectively maintained at 130 °C and 150 °C. The ρ_g value (in Eq. (22)) was calculated based on the composition of CH_4 (ca. 87%) and CO_2 (ca. 13%) in the metabolic gas. The pressure drop from the bottom of the reactor to the top of the fluidized bed was measured with a device (Druck STX 2100) that automatically recorded measurements electronically for subsequent computer analysis.

3.3. Hydrodynamic experiments

After completing all of the analytical work for the steady-state TAFBR operation, hydrodynamic experiments were conducted both with and without metabolic gas production for 5–9 different u_{l0} values (u_{l0} = 1.47–14.51 cm s^{-1}, $u_{g0} = 2.09 \times 10^{-2}$ to 8.38×10^{-2} cm s^{-1}, 17 sets for $\theta = 2.5°$; u_{l0} = 1.47–10.17 cm s^{-1}, $u_{g0} = 2.07 \times 10^{-2}$ to 8.38×10^{-2} cm s^{-1}, 19 sets for $\theta = 5°$, Table 2). In the experiments performed without metabolic gas production, the feeding of substrate was stopped, and the reactor liquid was continuously recycled until all of the residual substrate was consumed (time for thinner and thicker biofilms, <4 and <8 HRTs, respectively) and all metabolic gas production had stopped. For each value of u_{l0} examined, the reactor was continuously operated for at least three HRTs before the bed height and pressure drop were measured.

3.4. Simulation of $H_{b,GLS}$ and $H_{b,LS}$

Details of the simulation of $H_{b,GLS}$ are described as follows:

(1) Assume a value of $H_{b,GLS}$.
(2) Compute the simulated V_p (Eq. (12)).
(3) Compute the experimental V_p (Eq. (13)).
(4) Compute the error between the simulated and the experimental values of V_p.
(5) If the error is not within an acceptable range, set a new value for $H_{b,GLS}$ in procedure (1) and reiterate the above procedures until the error is accepted and the simulated $H_{b,GLS}$ is determined.

The simulated $H_{b,LS}$ is calculated in a manner similar to that described for the above procedures, while the ε_f in Eq. (13) is replaced by $\varepsilon_{l,LS}$.

4. Results and discussion

4.1. n, v_i, δ_0, m, and k

The operational parameters for the two tapered AFBRs and the corresponding steady-state experimental biofilm thickness are shown in Table 1 and Table 3, respectively. Values for n and v_i were obtained from regression analysis of the hydrodynamic data in the absence of metabolic gas production (Table 4). Both n and v_i increased with increasing δ_a, as did the biofilm thickness at the bottom of the reactor (δ_0) and the linear proportionality constant (m). The biofilm on the upper part of the fluidized beds was found to be thicker in both types of reactors. Similar results were reported by Hermanowicz and Cheng [6] and by Huang et al. [1].

In the present study, two tapered AFBRs producing metabolic gas, were used to generate hydrodynamic experimental data for the development of a correlation equation for k. MATLAB software [20], together with its "fzero" command, was used to solve Eq. (1) for k. After a value for k was determined, an inverse matrix was constructed to derive correlation equations for k, u_l, and u_g [21] using MATLAB. The results were as follows:

$$k = 0.0787 u_l^{1.699} u_g^{-0.699} \quad (\theta = 2.5°) \tag{26a}$$

$$k = 0.0029 u_l^{0.027} u_g^{-1.824} \quad (\theta = 5°) \tag{26b}$$

4.2. Hydrodynamic bed-expansion behavior

4.2.1. Experimental results

In order to explore the hydrodynamic bed-expansion behavior of the tapered AFBs, 36 sets of hydrodynamic experiments were conducted with metabolic gas production (Table 2), and 36 sets of experiments were conducted without metabolic gas production (i.e., the same operating ranges for u_{l0} as above, and $u_{g0} = 0$) (Fig. 2). Over the course of the experiments, the two tapered AFBRs were maintained in their fully fluidized states. The measured three-phase bed height, $H_{b,GLS}$, was slightly higher (by 1.8 ± 1.8%) than the corresponding two-phase bed height, $H_{b,LS}$, at a given value of u_{l0}. This implies that metabolic gas production causes slight bed expansion in the tapered AFBs. We speculated that the metabolic gas bubbles were trapped by the bioparticles, thereby lowering the particles' specific gravity. On the hydrodynamic bed-expansion behavior of conventional AFBRs (δ_a = 15–126 μm, $u_{g0} = 3.5 \times 10^{-3}$ to 14×10^{-3} cm s^{-1}; u_{l0} = 0.2–1.35 cm s^{-1}; Q_r = 8.4–48.6 l h^{-1}), the measured value for $H_{b,GLS}$ was 6.7 ± 5.5% higher than that for $H_{b,LS}$ for a given value for u_{l0} [8]. The three-phase bed volume, $V_{b,GLS}$, and its two-phase counterpart, $V_{b,LS}$, were calculated, and the

Table 3
Experimental biofilm thickness for three-phase tapered AFBRs

Run	θ (°)	Experimental δ (μm)			
		Lower part	Middle part	Upper part	Average
1	2.5	26	–	41	38
2	2.5	41	60	80	73
3	2.5	110	140	173	146
4	5.0	26	–	40	39
5	5.0	34	–	51	55
6	5.0	60	75	93	83

Table 4
Estimated results of n, v_i, δ_0, and m values

Run	θ (°)	n (–)	v_i (cm s^{-1})	δ_0 (μm)	m (μm)
1	2.5	2.923	3.43	11.4	41.3
2	2.5	5.873	4.79	21.9	76.1
3	2.5	6.245	9.52	43.8	149.3
4	5.0	2.365	3.33	11.7	40.8
5	5.0	3.794	4.22	16.5	56.6
6	5.0	13.885	14.76	24.9	82.0

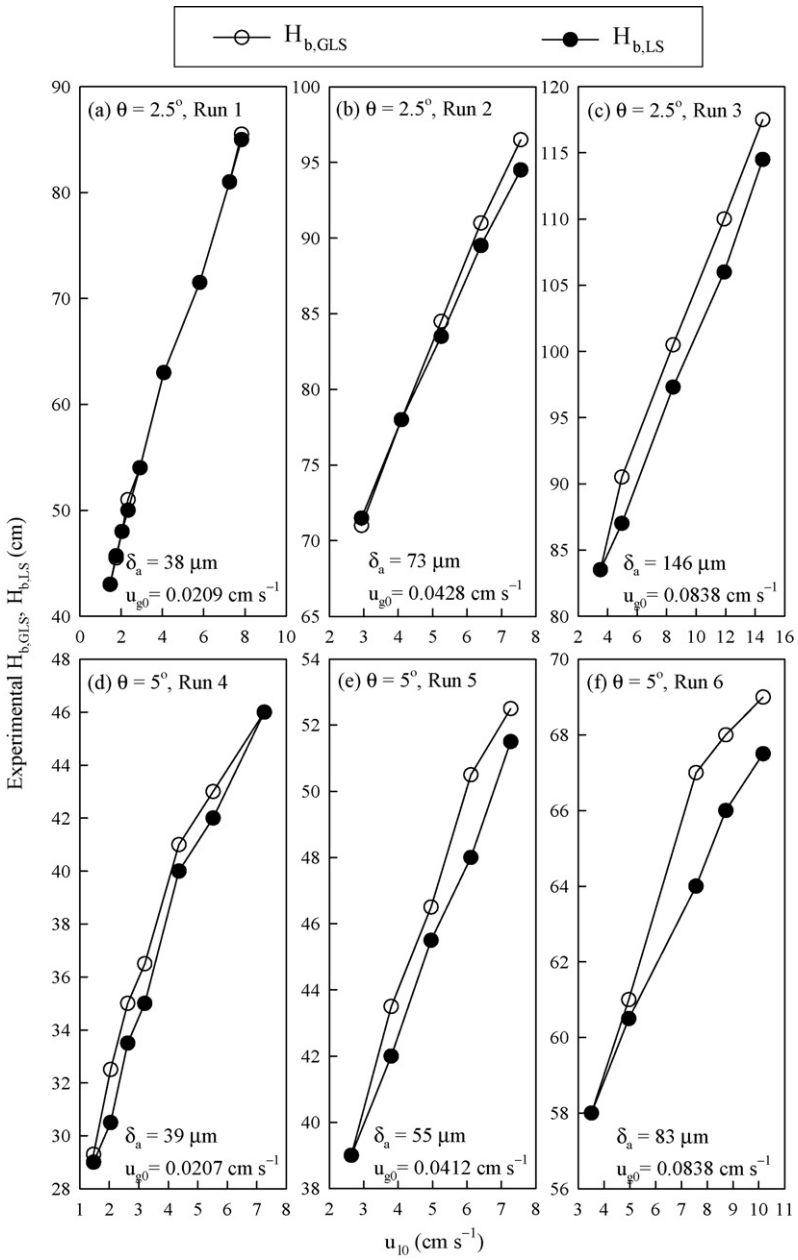

Fig. 2. Variations in experimental $H_{b,GLS}$ and $H_{b,LS}$ at different values of u_{l0}.

hydrodynamic bed-expansion behavior of tapered AFBRs was compared with that of conventional AFBRs. For the conventional AFBRs ($\delta_a = 126\ \mu m$, $u_{g0} = 0.014\ cm\ s^{-1}$, $u_{l0} = 1.07\ cm\ s^{-1}$, $Q_r = 38.6\ l\ h^{-1}$), the $V_{b,GLS}$ was approximately 7.5% higher than the corresponding $V_{b,LS}$. In contrast, for the tapered AFBRs ($\theta = 2.5^\circ$, $\delta_a = 73\ \mu m$, $u_{g0} = 0.0428\ cm\ s^{-1}$, $u_{l0} = 5.25\ cm\ s^{-1}$, $Q_r = 108.8\ l\ h^{-1}$; $\theta = 5^\circ$, $\delta_a = 83\ \mu m$, $u_{g0} = 0.0838\ cm\ s^{-1}$, $u_{l0} = 4.96\ cm\ s^{-1}$, $Q_r = 102.8\ l\ h^{-1}$), the $V_{b,GLS}$ values for both the $\theta = 2.5^\circ$ reactor and the $\theta = 5^\circ$ reactor were approximately 2.3% and 1.8% higher than the corresponding $V_{b,LS}$ values, respectively. In other words, production of metabolic gas produces a smaller bed expansion in tapered AFBs. This suggests that the operational stability of these reactors is greater than that of conventional AFBRs, especially at larger values of θ.

4.2.2. Model simulation

4.2.2.1. Different u_{l0}. Model simulations for predicting $H_{b,GLS}$ and $H_{b,LS}$ were performed using the following set of parameters: $u_{l0} = 4.1–14.5\ cm\ s^{-1}$, $u_{g0} = 0.08\ cm\ s^{-1}$, $\delta_a = 80\ \mu m$, $M_m = 200\ g$, $d_m = 633\ \mu m$, and k (Eqs. (26a) and (26b)). For reactor simulations with $\theta = 2.5^\circ$, the following values were used: $n = 5.909$, $v_i = 5.24\ cm\ s^{-1}$, $\delta_0 = 24.0\ \mu m$, and $m = 83.1\ \mu m$. For reactor simulations with $\theta = 5^\circ$, the following values were used: $n = 12.804$, $v_i = 13.63\ cm\ s^{-1}$, $\delta_0 = 24.9\ \mu m$, and $m = 79.3\ \mu m$. The values for n, v_i, δ_0, and m at $\delta_a = 80\ \mu m$ were obtained by performing a linear extrapolation of the available data (Table 4). The simulations predicted that the $H_{b,GLS}$ for the $\theta = 2.5^\circ$ and 5° reactors would be slightly higher ($2.59 \pm 0.68\%$) than the corresponding $H_{b,LS}$ (Fig. 3(a)). Thus, the simulated results regarding the effects of metabolic gas production on bed expansion within tapered AFBRs were in good agreement with experiment.

4.2.2.2. Different u_{g0}. In tapered AFBRs, the metabolic gas production rate generally increases with increasing biofilm thickness. The following correlation equations for δ_a and u_{g0} were generated

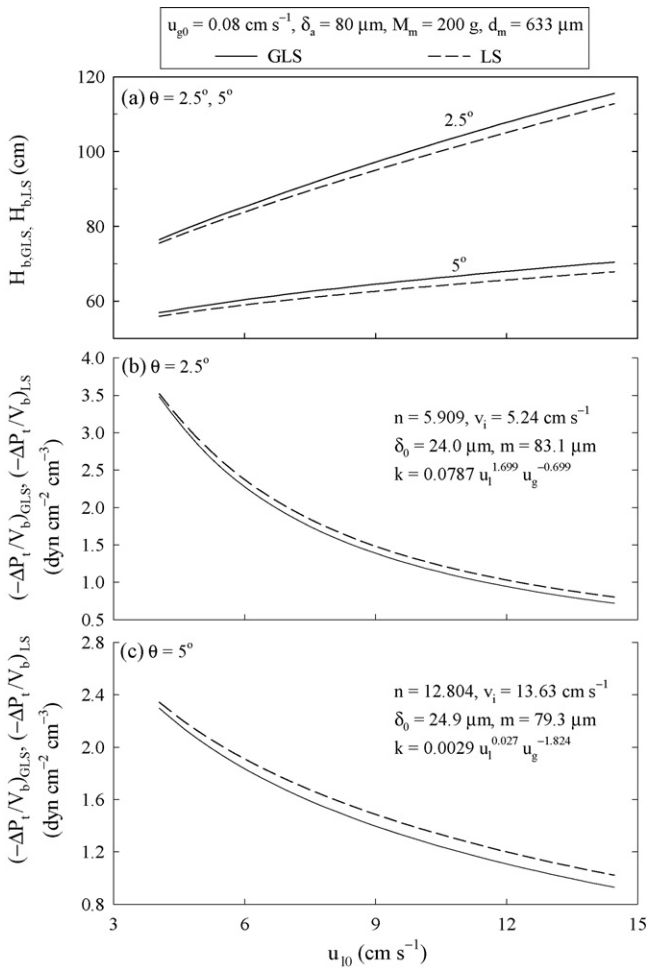

Fig. 3. Variations in simulated (a) $H_{b,GLS}$ and $H_{b,LS}$; (b) $\theta = 2.5^\circ$, $(-\Delta P_t/V_b)_{GLS}$ and $(-\Delta P_t/V_b)_{LS}$; (c) $\theta = 5^\circ$, $(-\Delta P_t/V_b)_{GLS}$ and $(-\Delta P_t/V_b)_{LS}$ at different values of u_{l0}.

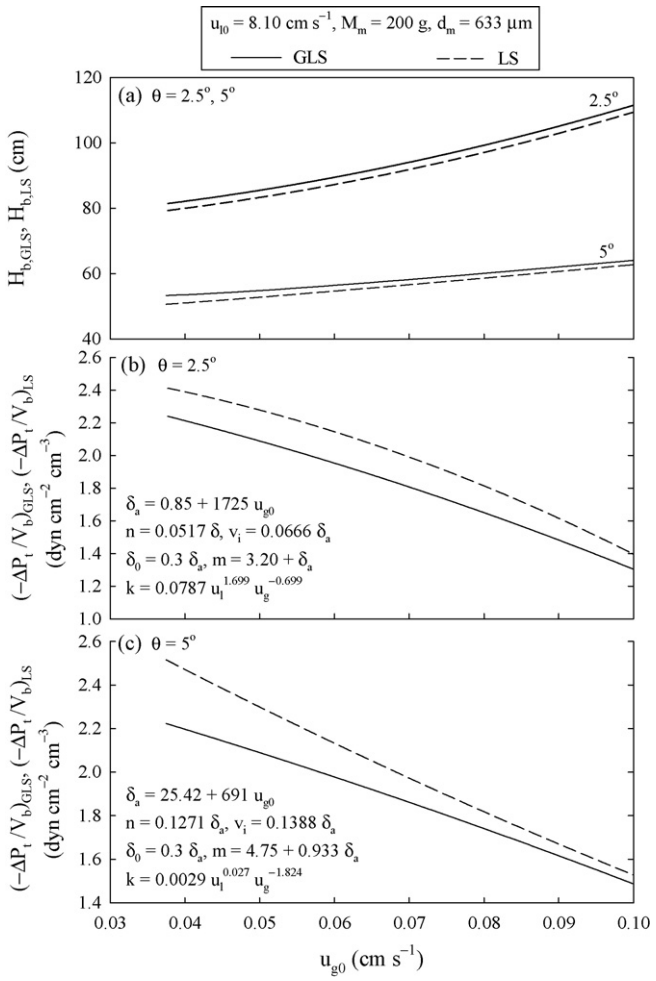

Fig. 4. Variations in simulated (a) $H_{b,GLS}$ and $H_{b,LS}$; (b) $\theta = 2.5^\circ$, $(-\Delta P_t/V_b)_{GLS}$ and $(-\Delta P_t/V_b)_{LS}$; (c) $\theta = 5^\circ$, $(-\Delta P_t/V_b)_{GLS}$ and $(-\Delta P_t/V_b)_{LS}$ at different values of u_{g0}.

through linear regression of the experimental data (Table 3):

$$\delta_a = 0.85 + 1725 u_{g0} \quad (\theta = 2.5^\circ) \tag{27a}$$

$$\delta_a = 25.42 + 691 u_{g0} \quad (\theta = 5^\circ) \tag{27b}$$

A similar linear regression combining the data for values n, v_i, δ_0, and m (Table 4) with the data for δ_a (Table 3) led to the following correlation equations:

(1) $\theta = 2.5^\circ$:

$$n = 0.0517\delta_a \tag{28a}$$

$$v_i = 0.0666\delta_a \tag{29a}$$

$$\delta_0 = 0.3\delta_a \tag{30a}$$

$$m = 3.20 + \delta_a \tag{31a}$$

(2) $\theta = 5^\circ$:

$$n = 0.1271\delta_a \tag{28b}$$

$$v_i = 0.1388\delta_a \tag{29b}$$

$$\delta_0 = 0.3\delta_a \tag{30b}$$

$$m = 4.75 + 0.933\delta_a \tag{31b}$$

All subsequent model simulations of $H_{b,GLS}$ and $H_{b,LS}$ were performed using Eqs. (28)–(31) and the following parameter values: $u_{l0} = 8.10\ \text{cm s}^{-1}$, $M_m = 200$ g, and $d_m = 633\ \mu\text{m}$. The value for k was determined from Eqs. (26a) and (26b), and u_{g0} was varied over the interval 0.038–0.10 cm s^{-1}. The simulated results show that the $H_{b,GLS}$ for the $\theta = 2.5^\circ$ reactor and the $\theta = 5^\circ$ reactor were slightly higher ($2.60 \pm 0.70\%$) than the corresponding $H_{b,LS}$ (Fig. 4(a)). Thus, metabolic gas production causes bed expansion effect in tapered AFBs, which is similar to the results with conventional AFBRs [8,9].

4.3. Hydrodynamic bed-pressure gradient

4.3.1. Experimental results

For a given reactor configuration and a given operating value for u_{l0}, the bed-pressure gradient is related to the specific energy-dissipation rate, such that the rate of biofilm detachment increases with an increasing specific energy-dissipation rate [10]. The bed-pressure drop $(-\Delta P_t)$ (Fig. 5) and the bed-pressure gradient $(-\Delta P_t/V_b)$ (Fig. 6) were measured during the hydrodynamic experiments on three-phase tapered AFBRs (the same operating range of u_{l0} and u_{g0} as those in Section 4.2.1) and two-phase tapered AFBRs (i.e., the same operating range of u_{l0} as above, and $u_{g0} = 0$). For the $\theta = 2.5^\circ$ reactor, the measured $(-\Delta P_t)_{GLS}$ value varied from 2839 to 6874 dyn cm^{-2} with an average of 4646 dyn cm^{-2}, while the $(-\Delta P_t/V_b)_{GLS}$ value varied from 0.90 to 13.98 dyn cm^{-2} cm^{-3} with an average of 4.68 dyn cm^{-2} cm^{-3}. The corresponding two-phase pressure drop $(-\Delta P_t)_{LS}$, varied from 2960 to 6898 dyn cm^{-2} with an average of 4756 dyn cm^{-2}, and the two-phase pressure gradient

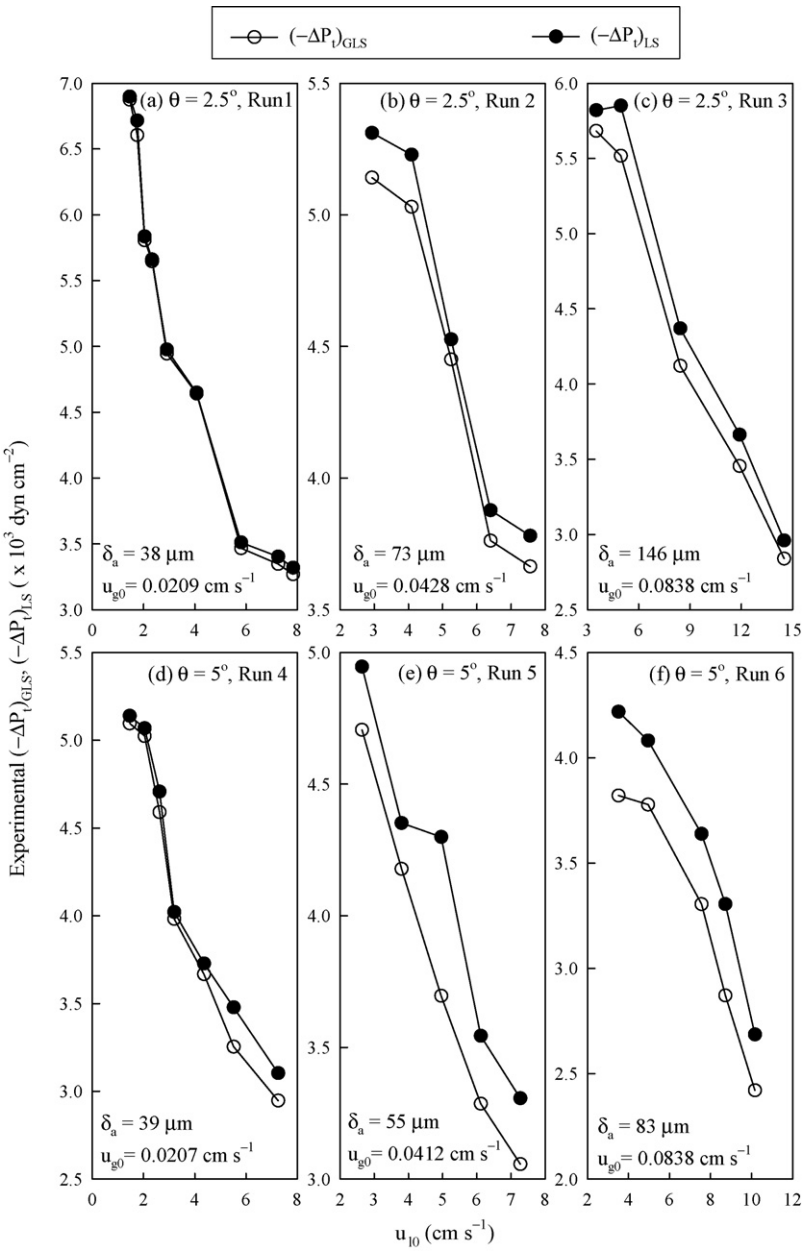

Fig. 5. Variations in experimental $(-\Delta P_t)_{GLS}$ and $(-\Delta P_t)_{LS}$ at different values of u_{l0}.

$(-\Delta P_t/V_b)_{LS}$, varied from 0.99 to 14.03 dyn cm^{-2} cm^{-3} with an average of 4.80 dyn cm^{-2} cm^{-3}. In other words, the measured $(-\Delta P_t)_{GLS}$ and $(-\Delta P_t/V_b)_{GLS}$ values were $2.4 \pm 1.9\%$ and $4.4 \pm 4.3\%$ lower than the corresponding $(-\Delta P_t)_{LS}$ and $(-\Delta P_t/V_b)_{LS}$ values, respectively. Both the measured $(-\Delta P_t)_{GLS}$ and $(-\Delta P_t/V_b)_{GLS}$ values decreased with increasing u_{l0}. Similarly, for the $\theta = 5^\circ$ reactor, the measured $(-\Delta P_t)_{GLS}$ and $(-\Delta P_t/V_b)_{GLS}$ values were $6.2 \pm 4.1\%$ and $10.8 \pm 4.8\%$ lower than the corresponding $(-\Delta P_t)_{LS}$ and $(-\Delta P_t/V_b)_{LS}$ values, respectively. On the hydrodynamic expansion characteristics of a conventional AFBR, in which $\delta_a = 15$–126 μm, $u_{l0} = 0.2$–1.35 cm s^{-1}, and $u_{g0} = 3.5 \times 10^{-3}$ to 14×10^{-3} cm s^{-1}, showed that the measured value for $(-\Delta P_t/V_b)_{GLS}$ was approximately $9.3 \pm 4.9\%$ lower than the corresponding value for $(-\Delta P_t/V_b)_{LS}$ [9]. The average $(-\Delta P_t/V_b)_{GLS}$ values for the TAFBRs (4.68 and 4.60 dyn cm^{-2} cm^{-3} for the $\theta = 2.5^\circ$ and 5° reactors, respectively) were lower than for the conventional AFBR (5.26 dyn cm^{-2} cm^{-3}). Thus, the thickening of the biofilm should be greater in tapered AFBRs than in conventional AFBRs, and this effect should be enhanced as the reactor's θ was increased. In general, the biofilm in the AFBRs was shallow, with a thickness of less than 300 μm. For the acetate substrate used in the shallow biofilm of AFBRs, the parameter of the effectiveness factor (i.e., the ratio of the substrate utilization rate within the biofilm to that without mass transfer resistance) approached unity. Also, the parameter of the Thiele modulus (ϕ^2) (i.e., the ratio of the substrate utilization rate to the substrate diffusion rate within the biofilm) fell within the reaction-controlled range ($\phi < 0.3$) [22]. These results reveal that the acetate methanogenesis reaction was reaction-controlled and that the biofilm was fully penetrated by the acetate substrate [23]. In other words, a thicker biofilm, which has a greater biomass, will benefit the performance of the AFBRs.

A thicker δ_a and a higher u_{g0}, corresponding to a higher rate of metabolic gas production, resulted in a lower bed-pressure gradient (Fig. 6). Both the measured and simulated values for $(-\Delta P_t)_{GLS}$ were close to the simulated value for $(-\Delta P_{flu})_{GLS}$, because the simulated

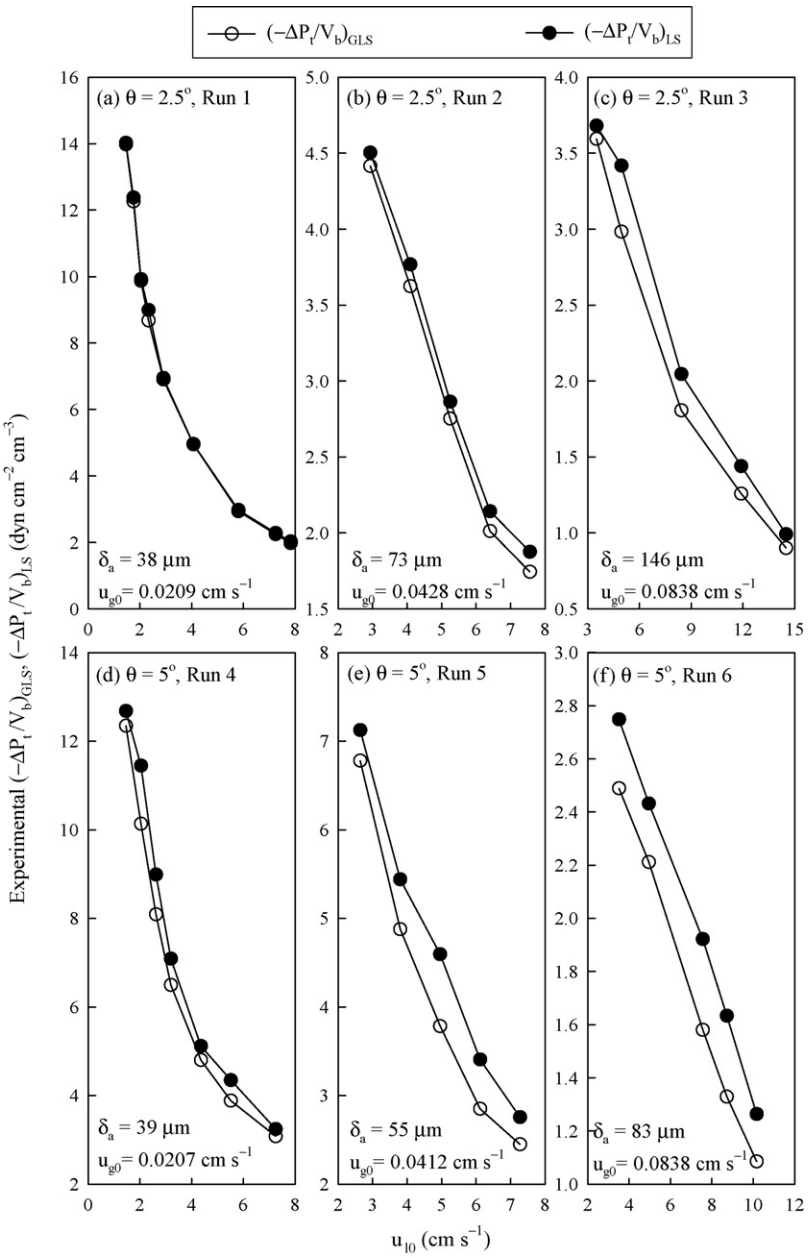

Fig. 6. Variations in experimental $(-\Delta P_t/V_b)_{GLS}$ and $(-\Delta P_t/V_b)_{LS}$ at different values of u_{l0}.

value for $|(-\Delta P_k)_{GLS}|$ contributed less than 0.3% to the simulated value for $(-\Delta P_t)_{GLS}$ (Table 5). The simulated value for $(-\Delta P_u)_{GLS}$ is zero, which verifies that the two tapered AFBRs were maintained in fully fluidized states.

4.3.2. Model simulation

4.3.2.1. Different u_{l0}. Using the parameter values from Section 4.2.2.1, simulations for the pressure gradient $(-\Delta P_t/V_b)_{GLS}$, in the fully fluidized state were performed to elucidate the relationship

Table 5
Experimental and simulated results of H_{GLS}, H_{LS}, $(-\Delta P_t)_{GLS}$, $(-\Delta P_t)_{LS}$, $(-\Delta P_{flu})_{GLS}$, and $(-\Delta P_k)_{GLS}$ of tapered AFBRs

Run	θ (°)	Experimental (cm)		Simulated (cm)		Experimental (dyn cm^{-2})		Simulated (dyn cm^{-2})[a]		
		H_{GLS}	H_{LS}	H_{GLS}	H_{LS}	$(-\Delta P_t)_{GLS}$	$(-\Delta P_t)_{LS}$	$(-\Delta P_{flu})_{GLS}$	$(-\Delta P_k)_{GLS}$	$(-\Delta P_t)_{GLS}$
1	2.5	51.0	50.0	49.1	48.6	5647	5661	6311	−2.8	6308
2	2.5	71.0	71.5	70.3	69.6	5141	5311	5121	−4.7	5116
3	2.5	83.5	83.5	82.0	81.0	5682	5820	5672	−7.7	5665
4	5.0	35.0	35.0	33.8	32.3	4590	4707	4919	−3.6	4915
5	5.0	39.0	39.0	38.6	37.9	4706	4946	4607	−4.1	4603
6	5.0	58.0	58.0	57.3	56.6	3821	4219	3450	−7.5	3442

[a] All simulated $(-\Delta P_u)_{GLS}$ values were 0.

between $(-\Delta P_t/V_b)_{GLS}$ and u_{l0}. For both the $\theta = 2.5^\circ$ (Fig. 3(b)) and $\theta = 5^\circ$ reactors (Fig. 3(c)), a higher u_{l0} resulted in a lower $(-\Delta P_t/V_b)_{GLS}$. This indicated that operating the tapered AFBR at a high u_{l0} may help to thicken the biofilm.

4.3.2.2. Different u_{g0}. Simulations of the three-phase pressure gradient $(-\Delta P_t/V_b)_{GLS}$, in the fully fluidized state were performed using the parameter values from Section 4.2.2.2, and the value for u_{g0} was varied over the range 0.038–0.100 cm s^{-1}. For both the $\theta = 2.5^\circ$ (Fig. 4(b)) and $\theta = 5^\circ$ reactors (Fig. 4(c)), a higher value for u_{g0} resulted in a lower value for $(-\Delta P_t/V_b)_{GLS}$, which led to a thickening of the biofilm. In addition, the simulated results (Figs. 4(b) and (c)) also showed that the three-phase gradient $(-\Delta P_t/V_b)_{GLS}$, is lower than the corresponding two-phase gradient $(-\Delta P_t/V_b)_{LS}$, offering further evidence that metabolic gas production induces biofilm thickening.

As metabolic gas bubbles attach to bioparticles, the specific gravity of the bioparticles will decrease, while the bed expansion volume will increase. On the one hand, the smaller momentum of the bioparticles, which results from their reduced specific gravity, will lessen their collision friction. On the other hand, the collision frequency among bioparticles will diminish because the particles become separated by metabolic gas bubbles. The attached metabolic gas bubbles play a buffering role, even though collisions among bioparticles still occur. Thus, the bed-pressure drop in the AFBR decreases. As a result, the $(-\Delta P_t/V_b)_{GLS}$ value is lower than $(-\Delta P_t/V_b)_{LS}$. These associations serve as a physical explanation for the relationship between biofilm thickening and metabolic gas production.

For thinner δ bioparticles, the described effect will be greater as metabolic gas bubbles attach to the particles because the specific gravity of the bioparticles will be lowered even more. A lower u_{g0} is given by thinner δ bioparticles. This is the reason why the difference between values of $(-\Delta P_t/V_b)_{GLS}$ and $(-\Delta P_t/V_b)_{LS}$ deviate more significantly at a lower u_{g0} (Figs. 4(b) and 4(c)).

4.4. Effect of taper angle

Simulations aimed at understanding the effects of taper angle on $H_{b,GLS}$, $H_{b,LS}$, $(-\Delta P_t/V_b)_{GLS}$, $(-\Delta P_t/V_b)_{LS}$, $\varepsilon_{l,GLS,a}$ and $\varepsilon_{g,a}$ were performed using the following set of parameter values: $u_{l0} = 8.10$ cm s^{-1}, $u_{g0} = 0.08$ cm s^{-1}, $\delta_a = 80$ μm, $M_m = 200$ g, $d_m = 633$ μm, $n = 5.848$, $v_i = 6.68$ cm s^{-1}, $\delta_0 = 21.7$ μm, $m = 74.4$ μm. The aforementioned values for n, v_i, δ_0, and m values were obtained by averaging the data in Table 4. The following correlation equation represents the average of Eqs. (26a) and (26b): $k = 0.0408 u_l^{0.863} u_g^{-1.2615}$. The taper angle, θ, was varied from 2.5° to 5°.

Both the three-phase and two-phase bed heights, $H_{b,GLS}$ and $H_{b,LS}$, decreased with increasing θ (Fig. 7a), implying that increasing θ may decrease the bioparticle washout rate. Again, $H_{b,GLS}$ was higher than the corresponding $H_{b,LS}$, indicating that metabolic gas production causes bed expansion in tapered AFBRs. The values for both $(-\Delta P_t/V_b)_{GLS}$ and $(-\Delta P_t/V_b)_{LS}$ decreased with increasing θ (Fig. 7b). This implies that increasing θ results in biofilm thickening. Once again $(-\Delta P_t/V_b)_{GLS}$ was lower than the corresponding $(-\Delta P_t/V_b)_{LS}$, meaning that metabolic gas production thickens the biofilm. Furthermore, both $\varepsilon_{l,GLS,a}$ and $\varepsilon_{g,a}$ decreased with increasing θ (Fig. 7b), resulting in a corresponding increase in $(1-\varepsilon_f)$ (Eq. (21)). Increasing θ increased the average cross-sectional area of the tapered AFBR, which in turn decreased $u_{l,a}$ and $u_{g,a}$. Nevertheless, the increase in θ was simultaneously associated with

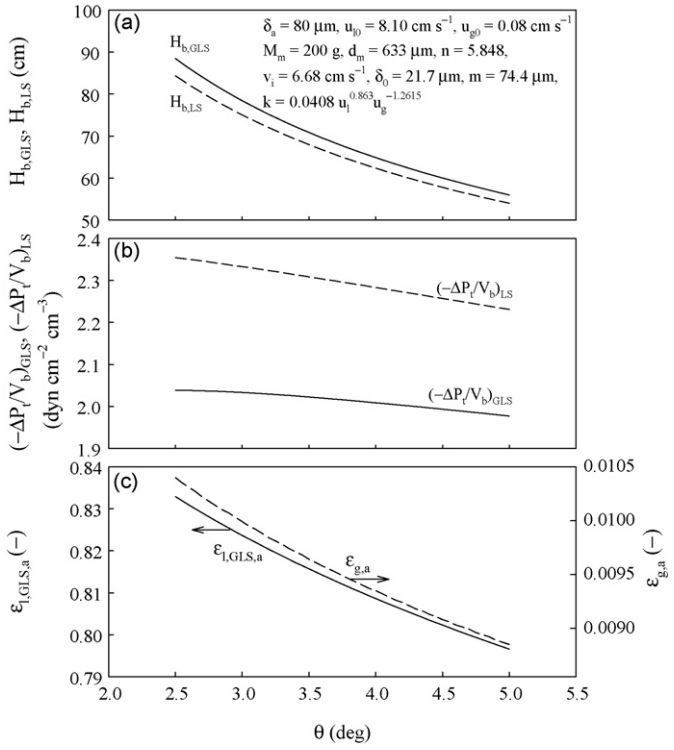

Fig. 7. Variations in simulated (a) $H_{b,GLS}$ and $H_{b,LS}$, (b) $(-\Delta P_t/V_b)_{GLS}$ and $(-\Delta P_t/V_b)_{LS}$, and (c) $\varepsilon_{l,GLS,a}$ and $\varepsilon_{g,a}$ at different values of θ.

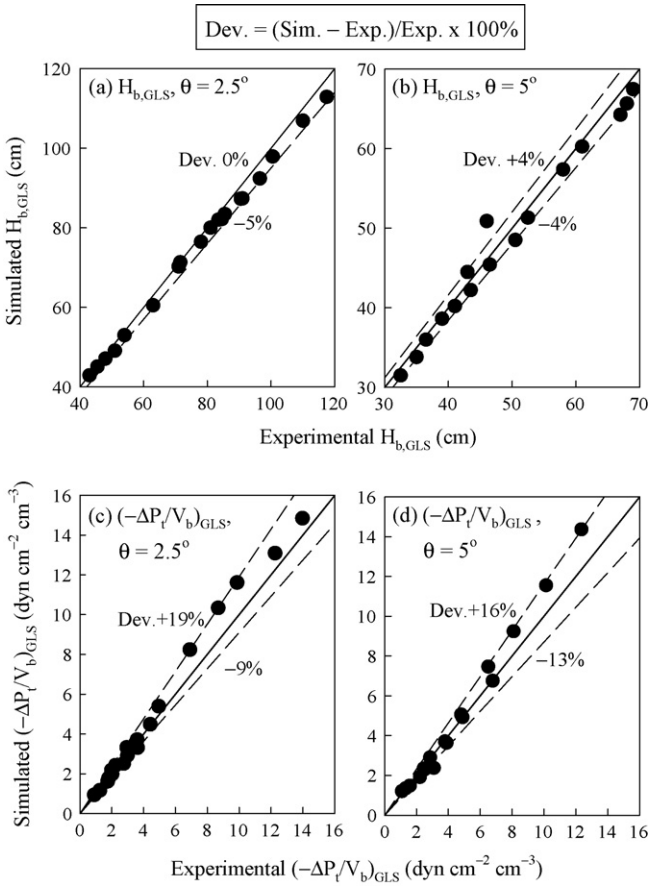

Fig. 8. Simulated vs. experimental (a) $H_{b,GLS}$, $\theta = 2.5^\circ$; (b) $H_{b,GLS}$, $\theta = 5^\circ$; (c) $(-\Delta P_t/V_b)_{GLS}$, $\theta = 2.5^\circ$; (d) $(-\Delta P_t/V_b)_{GLS}$, $\theta = 5^\circ$.

decreasing bed height, $H_{b,GLS}$, which compensated for the increased value for $(1-\varepsilon_f)$. Consequently, the values of both $(-\Delta P_{flu})_{GLS}$ and $(-\Delta P_t/V_b)_{GLS}$ decreased.

4.5. Model validation

The simulated values deviated from the experimental measurements of $H_{b,GLS}$ for the $\theta = 2.5^\circ$ and 5° reactors and they were in the range of (−5%)–(0%) and (−4%)–(+4%), respectively (Fig. 8(a) and (b)), while those of $(-\Delta P_t/V_b)_{GLS}$ for the $\theta = 2.5^\circ$ and 5° reactors were in the range of (−9%)–(+19%) and (−13%)–(+16%), respectively (Fig. 8(c) and (d)). The average relative errors between the simulated and the experimental values (i.e., (|sim. − exp.|/exp.) × 100%/number of test run) of $H_{b,GLS}$ and $(-\Delta P_t/V_b)_{GLS}$ were 2.64 ± 1.79% and 8.29 ± 6.04%, respectively. We therefore conclude that the proposed models adequately describe the hydrodynamic behavior of three-phase tapered AFBRs during metabolic gas production. Compared with the simulation of $H_{b,GLS}$, the simulation of $(-\Delta P_t/V_b)_{GLS}$ involved more parameters, such as Z_u, Z_{tr}, u_{mf}, ε_{mf}, and ρ_f, and more equations, which required greater calculation time. Thus, there was opportunity for more error and more error propagation. This resulted in poorer agreement between the simulated values and the experimental measurements for $(-\Delta P_t/V_b)_{GLS}$ than was observed for $H_{b,GLS}$.

5. Conclusions

In order for a model to adequately describe the hydrodynamic behavior of three-phase tapered AFBRs, wake theory, hydrostatic pressure, biofilm thickness distribution, and ambient temperature must all be taken into account. Metabolic gas production should also be considered. The proposed models adequately describe the hydrodynamic behavior of three-phase tapered AFBRs during metabolic gas production.

In tapered AFBRs in their fully fluidized states, the experimental and simulated results found when u_{l0} was varied at constant u_{g0}, and when u_{g0} was varied at constant u_{l0}, the $H_{b,GLS}$ was higher than the corresponding $H_{b,LS}$, implying that metabolic gas production induces bed expansion in tapered AFBs. The three-phase pressure gradient $(-\Delta P_t/V_b)_{GLS}$, was lower than the corresponding two phase gradient $(-\Delta P_t/V_b)_{LS}$. Both a higher u_{l0} for a given u_{g0} and a higher u_{g0} for a given u_{l0} resulted in a lower pressure gradient $(-\Delta P_t/V_b)_{GLS}$. Thus, the metabolic gas production induces biofilm thickening, especially at higher values of u_{l0} and u_{g0}. We suggest that the characteristics of bioparticles will change during processing. More specifically, during the process of bioparticle movement in the AFBRs, the specific gravity of bioparticles will decrease as the newly produced metabolic gas bubbles attach to them; the bed volume will increase; and the momentum of bioparticle collisions will diminish. In addition, the produced metabolic gas bubbles in the fluid buffer the collision momentum and separate the bioparticles, thereby lessening the collision frequency among bioparticles. Furthermore, the increased bed volume will further separate bioparticles and lower the collision frequency. As a result, the produced metabolic gas may promote thickening of the biofilm. In addition, increasing the value of θ, resulted in a decrease in $H_{b,GLS}$, which offset the increase in $(1-\varepsilon_f)$. Consequently, the value of $(-\Delta P_t/V_b)_{GLS}$ decreased with increasing θ.

Both experimental measurements and simulated predictions confirm that TAFBRs should be superior to conventional AFBRs in terms of operational stability and biofilm thickening, particularly for reactors with larger taper angles.

Acknowledgements

Financial support from the National Science Council of the Republic of China (Taiwan) is greatly appreciated (grants NSC 92-2211-E-426-001 and NSC 94-2211-E-426-002).

References

[1] J.S. Huang, J.L. Yan, C.S. Wu, Comparative bioparticle and hydrodynamic characteristics of conventional and tapered anaerobic fluidized-bed bioreactors, J. Chem. Technol. Biotechnol. 75 (2000) 269–278.
[2] V.K. Bhatia, N. Epstein, Three phase fluidization: a generalized wake model, in: H. Angelino, J.P. Couderc, H. Gibert, C. Laguerie (Eds.), Fluidization and Its Applications, Cepadues-Editions, Toulouse, 1974, p. 372.
[3] S.A. El-Temtamy, N. Epstein, Bubble wake solids content in three-phase fluidized beds, Int. J. Multiphase Flow 4 (1978) 19–31.
[4] S.H. Chern, L.S. Fan, K. Muroyama, Hydrodynamics of concurrent gas–liquid–solid semifluidization with a liquid as the continuous phase, AIChE J. 30 (1984) 288–294.
[5] L.S. Fan, A. Matsuura, S.H. Chern, Hydrodynamic characteristics of a gas–liquid–solid fluidized bed containing a binary mixture of particles, AIChE J. 31 (1985) 1801–1810.
[6] S.W. Hermanowicz, Y.W. Cheng, Biological fluidized bed reactor: hydrodynamics, biomass distribution and performance, Water Sci. Technol. 22 (1990) 193–202.
[7] T. Setiadi, Predicting the bed expansion of an anoxic fluidized-bed bioreactor, Water Sci. Technol. 31 (1995) 181–191.
[8] C.S. Wu, J.S. Huang, H.Y. Gou, Expansion characteristics of an anaerobic fluidized bed reactor with internal biogas production, J. Chem. Technol. Biotechnol. 80 (2005) 1273–1281.
[9] C.S. Wu, J.S. Huang, H.H. Chou, Influence of internal biogas production on hydrodynamic behavior of anaerobic fluidized-bed reactors, Water Res. 40 (2006) 126–136.
[10] J.S. Huang, C.S. Wu, Specific energy dissipation rate for fluidized-bed bioreactors, Biotechnol. Bioeng. 50 (1996) 643–654.
[11] Y. Kato, T. Uchida, T. Kago, S. Morooka, Liquid hold-up and heat transfer coefficient between bed and wall in liquid–solid and gas–liquid–solid fluidized beds, Powder Technol. 28 (1981) 173–179.
[12] H.T. Chang, B.E. Rittmann, Predicting bed dynamics in three-phase fluidized-bed biofilm reactors, Water Sci. Technol. 29 (1994) 231–241.
[13] H. Yu, B.E. Rittmann, Predicting bed expansion and phase hold-ups for three-phase fluidized-bed reactors with and without biofilm, Water Res. 31 (1997) 2604–2616.
[14] A.R. Khan, J.F. Richardson, The resistance to motion of a solid sphere in a fluid, Chem. Eng. Commun. 62 (1987) 135–150.
[15] A.R. Khan, J.F. Richardson, Fluid-particle interactions and flow characteristics of fluidized beds and settling suspensions of spherical particles, Chem. Eng. Commun. 78 (1989) 111–130.
[16] P. Buffière, C. Fonade, R. Moletta, Mixing and phase hold-ups variations due to gas production in anaerobic fluidized-bed digesters: influence on reactor performance, Biotechnol. Bioeng. 60 (1998) 36–43.
[17] Y. Peng, L.T. Fan, Hydrodynamics characteristics of fluidization in liquid–solid tapered beds, Chem. Eng. Sci. 52 (1997) 2277–2290.
[18] H.H. Chou, J.S. Huang, W.F. Hong, Temperature dependency of granule characteristics and kinetic behavior in UASB reactors, J. Chem. Technol. Biotechnol. 79 (2004) 797–808.
[19] W.K. Shieh, P.M. Sutton, P. Kos, Predicting reactor biomass concentration in a fluidized-bed system, J. WPCF 53 (1981) 1574–1584.
[20] C. Moler, Matlab Version 7.0, Release 14, The MathWorks Inc., Natick, MA, 2005.
[21] M.E. Herniter, Programming in Matlab, Brooks/Cole, Thomson Learning, CA, 2001.
[22] J.E. Bailey, D.F. Ollis, Biochemical Engineering Fundamentals, 2nd ed., McGraw-Hill, New York, 1986, pp. 202–220.
[23] C.S. Wu, J.S. Huang, Bioparticle characteristics of tapered anaerobic fluidized-bed bioreactors, Water Res. 30 (1996) 233–241.